# Infrared and visible image fusion using Latent Low-Rank Representation

Hui Li, Xiao-Jun Wu

Abstract-Infrared and visible image fusion is an important problem in the field of image fusion, and has been applied widely in many fields. To better preserve the useful information from infrared and visible images, in this paper, we propose a novel image fusion method based on latent low-rank representation (LatLRR) which is simple and effective. This is the first time that the LatLRR is introduced to infrared and visible image fusion. Firstly, the source images are decomposed into low-rank part and saliency part by LatLRR. The global structure information is preserved by low-rank part, and the local structure information is extracted by saliency part. Then, the low-rank parts are fused by weighted-average strategy, and the saliency parts are simply fused by sum strategy. Finally, the fused image is obtained by combining the fused low-rank part and the fused saliency part. Compared with other fusion methods experimentally, the proposed method has better fusion performance than the state of the art fusion methods in both subjective and objective evaluation.

Index Terms—image fusion, latent low-rank representation, infrared image, visible image.

### I. Introduction

In multi-sensor image fusion field, the infrared and visible image fusion is a very important task. It has been widely used in many applications, such as surveillance, object detection and target recogintion. The main purpose of image fusion is to generate a single image which contains the complementary information from multiple images of the same scene[1]. In infrared and visible image fusion, it is a key problem to extract the saliency object from infrared image and visible image. And many fusion methods have been proposed in recently.

As we all know, the most commonly used method in image fusion are multi-scale transforms, such as discrete wavelet transform(DWT)[2], contourlet trnsform[3], shift-invariant shearlet transform[4] and quaternion wavelet transform[5] etc. Due to the conventional tansform methods has not enough detail preservation ability, Lou et al.[6] proposed a fusion method based on contextual statistical similarity and nonsubsampled shearlet transform which can obtain the local structure information from source image and get good fusion performance. For infrared and visible image fusion, B.P. Bavirisetti et al.[7] proposed a fusion method based on two-scale decomposed and saliency detection, they used mean filter and median filter to extract the base layers and detail layers, and used visual saliency to obtain weight maps. Finally, the fused image is obtained by calculating these three parts. Besides

above methods, Yu Zhang et al.[8] proposed a morphological gradient based fusion method. This method used the different morphological gradient operator to obtain the focus region, defocus region and focus boundary region, respectively. Then the fused image is obtained by using an appropriate fusion strategy.

Recently, with the rise of compressed sensing, image fusion methods based on representation learning has attracted great attention. The most common methods of representation learning are sparse representation(SR). Zong J.J. et al.[9] proposed a novel medical image fusion method based on SR. They used the Histogram of Oriented Gradient(HOG) features to classify the image patches and learned several sub-dictionaries. Then this method used the  $l_1$ -norm and choose-max strategy to reconstruct fused image. In addition, there are many methods based on combining SR and other tools which are pulse coupled neural network(PCNN)[10] and shearlet transform[11]. In sparse domain, the joint sparse representation[12], convolutional sparse representation[13] and cosparse representation[14] were also applied into image fusion field.

Although the SR based fusion methods obtain good fusion performance, these methods still have drawback, such as the ability of capturing global structure is limited. To address this problem, we introduce a new representation learning technique, latent low-rank representation (LatLRR)[15], to infrared and visible image fusion task. Unlike low-rank representation(LRR)[16], the LatLRR can extract the global structure information and the local structure information from source images.

In this paper, we propose a novel fusion method based on LatLRR in infrared and visible image fusion which is simple and effective. The source images are decomposed into low-rank parts and saliency parts by LatLRR. Where the global structure information is preserved by low-rank part, and the local structure information is extracted by saliency part. Then the fused low-rank part is obtained by weighted-average strategy, and the fused saliency part is obtained by sum strategy. Finally, we use fused low-rank part and fused saliency part to reconstruct the fused image. And the experimental results demonstrate that our proposed has better fusion performance than other fusion methods.

This paper is structured as follows. In Section II, we give a brief introduction to LatLRR theory. In Section III, the proposed LatLRR based image fusion method is introducted in detail. The experimental results are shown in Section IV. Finally, Section V draws the conclusions.

H. Li is with the School of Internet of Things Engineering, Jiangnan University, Wuxi 214122, China.

X. Wu is with the School of Internet of Things Engineering, Jiangnan University, Wuxi 214122, China. e-mail: xiaojun\_wu\_jnu@163.com

### II. LATENT LOW-RANK REPRESENTATION THEORY

In 2010, Liu G.C. et al.[16] proposed LRR theroy, but this representation method can not preserve the local structure information. So in 2011, the author proposed LatLRR theroy[15], and the global structure and local structure can be extracted by LatLRR from raw data.

In reference [16], the LatLRR problem is reduced to solve the following optimization problem,

$$\min_{Z,L,E} ||Z||_* + ||L||_* + \lambda ||E||_1 
s.t., X = XZ + LX + E$$
(1)

where  $\lambda>0$  is the balance coefficient,  $||\cdot||_*$  denotes the nuclear norm which is the sum of the singular values of matrix and  $||\cdot||_1$  is  $l_1$ -norm. X denotes observed data matrix, Z is the low-rank coefficients, L is the saliency coefficients, and E is the sparse noisy part. Eq.(1) is solved by the inexact Augmented Lagrangian Multiplier (ALM). Then the low-rank part XZ and the saliency part LX is obtained by Eq.(1).

# III. THE PROPOSED FUSION METHOD

In this section, the proposed fusion method is presented in detail. And the fusion processing of low-rank parts and saliency parts will be introduced in next sections.

The LatLRR decomposed operation is shown in Fig.1. The low-rank part and saliency part for input image are obtained by LatLRR.

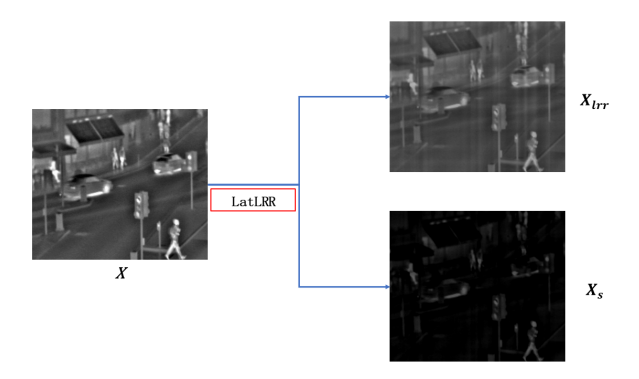


Fig. 1. The LatLRR decomposed operation.

As shown in Fig.1, X is the input image,  $X_{lrr} = XZ$  and  $X_s = LX$  denote the low-rank part and saliency part which are obtained by LatLRR. When we get the low-rank parts and saliency parts from each source images, we will use fusion strategy to fusedd these two parts, respectively. And the framework of the proposed fusion method is shown in Fig.2.

The two source images are donated as  $I_1$  and  $I_2$ . Firstly, the low-rank part  $I_{C\_lrr}$  and saliency part  $I_{C\_s}$  for each source image are obtained by LatLRR, where  $C \in \{1,2\}$ . Then the low-rank parts and saliency parts are fused by weighted-average strategy, respectively. Finally, the fused image F will be reconstructed by adding the fused low-rank part  $F_lrr$  and saliency part  $F_s$ .

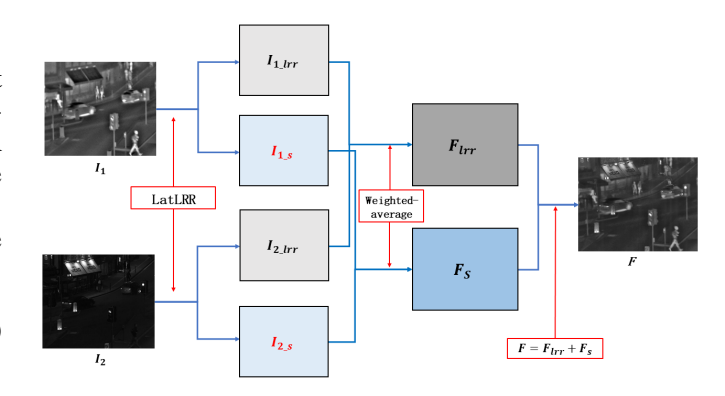


Fig. 2. The framework of proposed method.

### A. Fusion of low-rank parts

The fusion procedure of low-rank parts is shown in Fig.3. The low-rank parts for source images contain more global structure information and brightness information. So, in our fusion method, we use weighted average strategy to obtain the fused low-rank part. The fused low-rank part is calculated by Eq.(2),

$$F_{lrr}(i,j) = w_1 I_{1\_lrr}(i,j) + w_2 I_{2\_lrr}(i,j)$$
 (2)

where (i,j) denotes the corresponding position of the coefficient in  $I_{1\_lrr}$ ,  $I_{2\_lrr}$  and  $F_{lrr}$ . And  $w_1$  and  $w_2$  represent the weight values for coefficient in in  $I_{1\_lrr}$  and  $I_{2\_lrr}$ , respectively. To preserve the global structure and brightness information, and to reduce the redundant information, in this paper, we choose  $w_1=0.5$  and  $w_2=0.5$ .

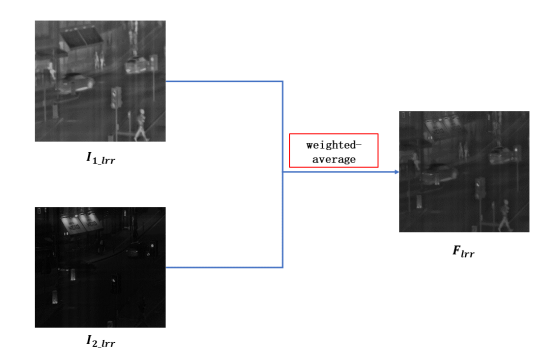


Fig. 3. The fusion procedure of low-rank parts.

### B. Fusion of saliency parts

The saliency parts are obtained by LatLRR from source images contain the local structure information and saliency features, as shown in Fig.4.

As we can see from the example in Fig.4, the saliency part  $I_{1\_s}$  contains more saliency features from  $I_1$  and it is the same situation for  $I_{2\_s}$  and  $I_2$ . The saliency features from source images are complementary information and need to be contained in fused images without loss. So in Eq.(3), we simply use sum strategy to fusedd the saliency parts.

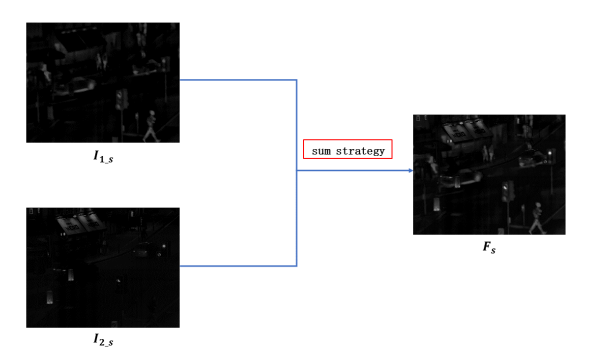


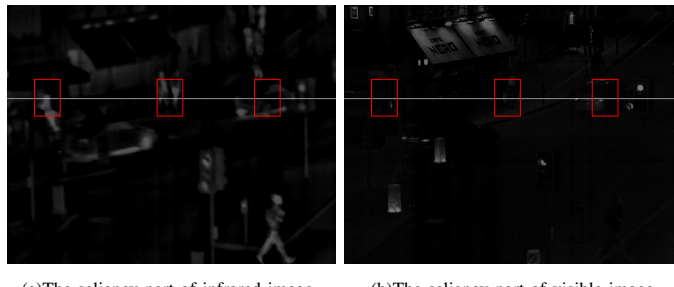
Fig. 4. The fusion procedure of saliency parts.

$$F_s(i,j) = s_1 I_{1\ s}(i,j) + s_2 I_{2\ s}(i,j) \tag{3}$$

In Eq.(3), the (i, j) represent the corresponding position of the coefficient in  $I_1$  s,  $I_2$  s and  $F_s$ . And  $w_1$  and  $w_2$ represent the weight value for coefficient in in  $I_1$  s and  $I_2$  s, respectively. To preserve more local structure and saliency features in fused images, in this paper, we choose  $s_1 = 1$ and  $s_2 = 1$  in Eq.(3). In next section, we will introduce why we use sum strategy and choose  $s_1 = s_2 = 1$ .

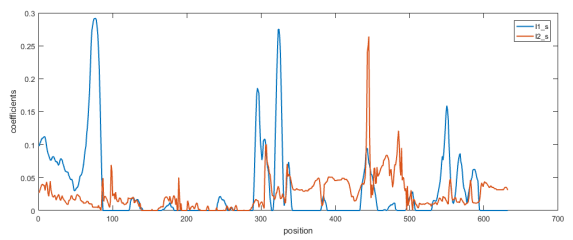
# C. The Reason of choose sum strategy

In this section, we will explain why we simply use the sum strategy to fused the saliency parts. We choose the coefficients from two saliency parts in same row, as shown in Fig.5(a) and Fig.5(b). Fig.5(c) indicate the saliency part values in the same row and different column.



(a)The saliency part of infrared image.

(b)The saliency part of visible image.

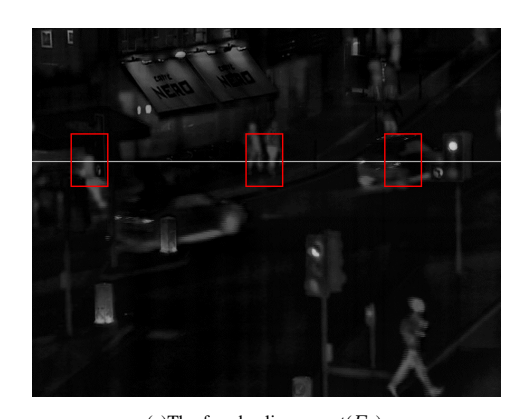


(c)The corresponding coefficients in same row and different column.

Fig. 5. Example of coefficients corresponding to the same row in infrared and visible saliency parts, (a) $I_{1\_s}$  and (b) $I_{2\_s}$  denote the saliency parts, (c) plot of two saliency parts values in same row.

As we can see in Fig.5(a) and Fig.5(b), the white line denotes the row which we choose in Fig.5(c). And in Fig.5(c), the blue line and orange line indicate the coefficients of infrared saliency part( $I_{1\ s}$ ) and visible saliency part( $I_{2\ s}$ ), respectively. From Fig.5(a) and Fig.5(b), in the first and second red boxes, the infrared saliency part contains more saliency features which means the coefficients of infrared saliency part are greater than visible saliency part in corresponding position and the values of visible saliency part are close to 0, as shown in Fig.5(c) and the position in [50, 100] and [250, 350]. In the third red box, the visible saliency part contains more saliency features, which means the coefficients of visible saliency part are greater than infrared saliency part in corresponding position and the values of infrared saliency part are very small, as shown in Fig.5(c) and the position in [400, 500].

The fused saliency part and the corresponding coefficients are shown in Fig.6. Fig.6(a) is the fused saliency part which use sum strategy, and the red line in Fig.6(b) indicate the coefficients of fused saliency part in same row.



(a) The fused saliency  $part(F_s)$ .

(b)The corresponding coefficients of fused saliency part in same row and different column.

Fig. 6. Example of coefficients corresponding to the same row in fused saliency parts, (a) the fused saliency parts, (b) plot of fused saliency parts values in same row.

As we discuss in Section B, the saliency features from source images need to be contained in fused images without loss. If we choose weight-average strategy, the saliency features will be reduced. And if we choose sum strategy to fusedd saliency part, the saliency features will be contained in fused saliency part without loss. Furthermore, the features will be increased by sum strategy, as shown in Fig.6(b).

# D. Reconstruction

When the fused low-rank part  $F_{lrr}$  and saliency part  $F_s$ are obtained by Eq.(2) and Eq.(3), the fused image F will be reconstructed by Eq.(4),

$$F(i,j) = F_{lrr}(i,j) + F_s(i,j) \tag{4}$$

# E. Summary of the Proposed Fusion Method

We summarize the proposed fusion method based on LatLRR as follows:

- 1) The source images are decomposed by LatLRR to obtain the low-rank parts  $I_{C\_lrr}$  and the saliency part  $I_{C\_s}$ , where  $C \in {1,2}$ .
- 2) We choose weighted-average fusion strategy to fused low-rank parts and saliency parts. Then the fused low-rank part  $F_{lrr}$  and the fused saliency part  $F_s$  are obtained.
  - 3) Finally, the fused image are obtained by Eq.(4).

### IV. EXPERIMENTAL RESULTS

In this section, first of all, we introduce the detailed experimental settings. Then the subjective and objective methods are adopted to assess the fusion performance. Finally, the experimental results are analyzed visually and quantitatively.

# A. Experimental Settings

Firstly, the source infrared and visible images were collected from https://figshare.com/articles/TNO\_Image\_Fusion\_Dataset/1008029 and the reference[17]. And the number of our source images are 21 pairs. Because the number of infrared and visible images are too much to show all of them, so we just take several examples for these images, as shown in Fig.(7).

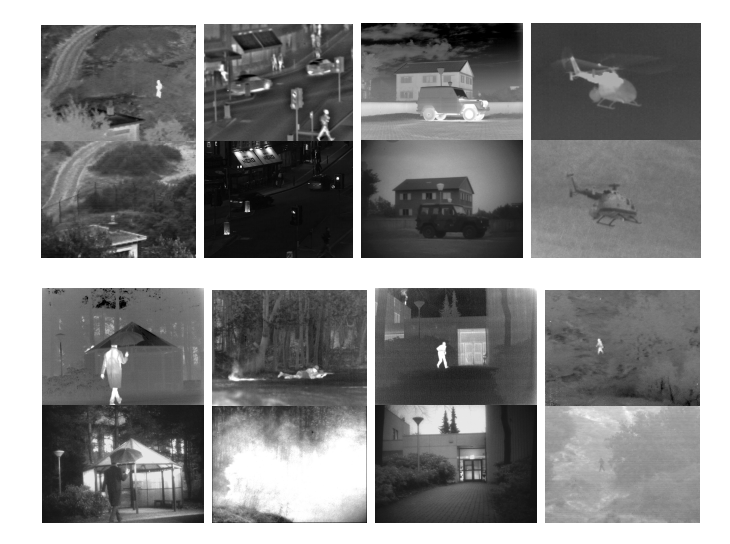


Fig. 7. Eight pairs of source images from 21 pairs.

Then several novel and classical fusion methods are compared with the proposed method, including: cross bilateral filter fusion method(CBF)[18], discrete cosine harmonic wavelet transform fusion method(DCHWT)[19], the joint-sparse representation model(JSR)[20], the JSR model with saliency detection fusion method(JSRSD)[12], and the gradient transfer fusion method(GTF)[21].

In our experiments, the parameter  $\lambda$  in LatLRR is 0.8. And the weighting value for fusing the low-rank parts is 0.5, the weighting value for fusing the saliency parts is 1. The evaluation methods for fusion performance will be introduced in next sections.

All the experiments are implemented in MTALAB R2016a on 3.2 GHz Intel(R) Core(TM) CPU with 12 GB RAM.

# B. Subjective Evaluation

The fusion results are obtained by five compared methods and proposed method are shown in Fig.(8-9), we just choose two pairs infrared and visible images(street and car) to assess the fusion performance by subjective evaluation.

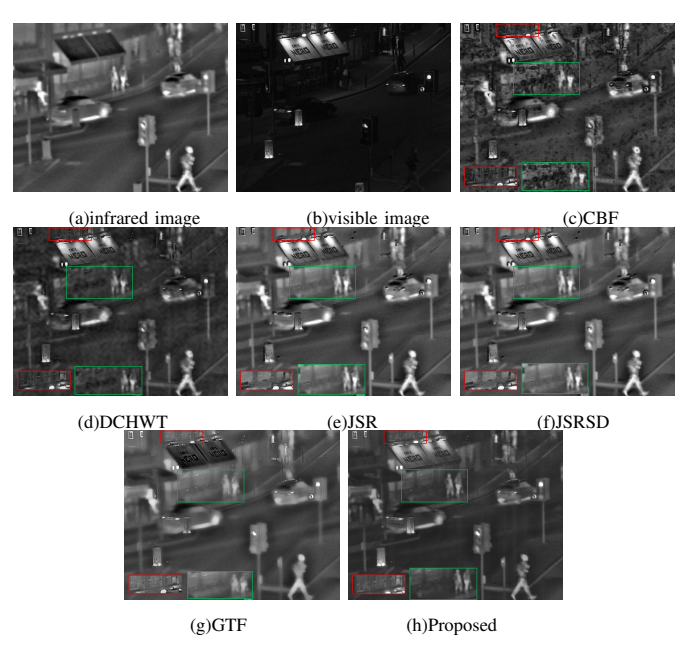


Fig. 8. Experiment on street images. (a) Infrared image; (b) Visible image; (c) The fused image obtained by CBF; (d) The fused image obtained by DCHWT; (e) The fused image obtained by JSR; (f) The fused image obtained by JSRSD. (g) The fused image obtained by GTF; (h) The fused image obtained by the proposed method.

As shown in Fig.(8) and Fig.(9), Fig.8(c-h) and Fig.9(c-h) are the fused images which are obtained by the compared fusion methods and the proposed fusion method. As we can see from the fused images in Fig.(8), the fused image which is obtained by proposed method can preserve more windows and chair detail information in red and green boxes, respectively. In Fig.(9), the fused image which is obtained by proposed method also contain more glass detail information in red box.

In summary, the fused images which are obtained by CBF and DCHWT have more artifacts information and the saliency features are not clear. For the fused images which are obtained by JSR, JSRSD and GTF contain many ringing artifacts around the saliency features and the detail information are also not clear. In contrast, the fused images which are obtained by proposed fusion method contain more saliency features and preserve more detail information. Compared with above fusion methods, the fused images which are obtained by proposed fusion method are more natural for human sensitivity and the proposed method has better subjective fusion performance.

### C. Objective Evaluation

For the purpose of quantitative comparison between the proposed method and other fusion methods, three quality metrics are utilized. These are:  $N_{abf}[19]$  which denotes the rate of noise or artifacts added in fused image due to fusion process, the sum of the correlations of differences(SCD)[22], and modified structural similarity( $SIM_a$ ).



Fig. 9. Experiment on car images. (a) Infrared image; (b) Visible image; (c) The fused image obtained by CBF; (d) The fused image obtained by DCHWT; (e) The fused image obtained by JSR; (f) The fused image obtained by JSRSD. (g) The fused image obtained by GTF; (h) The fused image obtained by the proposed method.

In our experiment, the  $SSIM_a$  is calculated by Eq.(5),

$$SSIM_a(F) = (SSIM(F, I_1) + SSIM(F, I_2)) \times 0.5$$
 (5)

where  $SSIM(\cdot)$  represents the structural similarity operation, F is fused image. And  $I_1$ ,  $I_2$  are source images. The value of  $SSIM_a$  denotes the ability of structural preservation.

The fusion performance of fused image is better with the increasing numerical index of SCD and  $SSIM_a$ . On the contrary, the fusion performance is better when the value of  $N_{abf}$  is small.

In this section, the values of  $N_{abf}$ , SCD and  $SSIM_a$  for 21 pairs source images are shown in three tables which are Table I, Table II and Table III respectively. And we use image1-21 to represent these source images. The average values of  $N_{abf}$ , SCD and  $SSIM_a$  are shown in Fig.(10-12) with histogram.

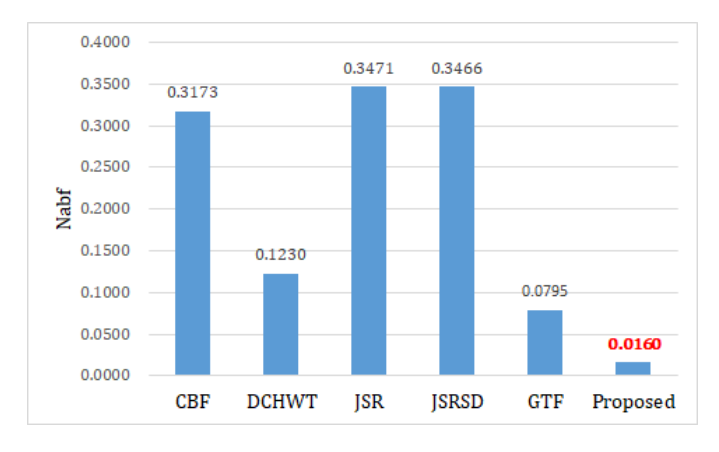


Fig. 10. The average values of  $N_{abf}$  for fusion methods.

In Table I, Table II and Table III, the best values for  $N_{abf}$ , SCD and  $SSIM_a$  are indicated in bold and the second-best

Methods	CBF	DCHWT	JSR	JSRSD	GTF	Proposed
image1	0.2317	0.0512	0.3415	0.3415	0.0703	0.0172
image2	0.4870	0.2184	0.1975	0.1989	0.1124	0.0292
image3	0.5448	0.2862	0.3863	0.3863	0.0734	0.0374
image4	0.4529	0.1909	0.4235	0.4235	0.1430	0.0208
image5	0.4326	0.0742	0.4980	0.4980	0.0850	0.0223
image6	0.2393	0.1027	0.3662	0.3651	0.0640	0.0087
image7	0.4178	0.1506	0.5230	0.5222	0.0525	0.0317
image8	0.1523	0.0578	0.2164	0.2154	0.1233	0.0112
image9	0.1174	0.0534	0.3098	0.3076	0.0901	0.0048
image10	0.2009	0.0927	0.3433	0.3427	0.1040	0.0059
image11	0.4763	0.1034	0.3322	0.3294	0.0732	0.0327
image12	0.2554	0.0726	0.3249	0.3250	0.0365	0.0140
image13	0.3607	0.0995	0.2811	0.2822	0.0658	0.0156
image14	0.1897	0.0858	0.4062	0.4026	0.0912	0.0080
image15	0.2151	0.0953	0.3511	0.3501	0.0752	0.0097
image16	0.5278	0.1841	0.2691	0.2689	0.0829	0.0214
image17	0.5289	0.1971	0.3354	0.3372	0.0328	0.0136
image18	0.2665	0.0688	0.5576	0.5573	0.0329	0.0071
image19	0.1258	0.0189	0.2733	0.2730	0.0416	0.0068
image20	0.2589	0.2451	0.1659	0.1654	0.0929	0.0091
image21	0.1809	0.1334	0.3873	0.3855	0.1268	0.0078

TABLE II THE SCD VALUES OF THE COMPARED METHODS AND THE PROPOSED METHOD FOR 21 pairs source images.

Methods	CBF	DCHWT	JSR	JSRSD	GTF	Proposed
image1	1.3044	1.4454	1.4111	1.4111	0.9689	1.7331
image2	1.2719	1.4368	1.7014	1.7029	1.1057	1.7387
image3	1.5629	1.8502	1.7467	1.7467	1.1387	1.9161
image4	1.4797	1.6059	1.5846	1.5846	0.9745	1.7493
image5	1.2718	1.4835	0.7489	0.7489	0.7037	1.4225
image6	1.3901	1.7113	1.7773	1.7776	1.0526	1.7991
image7	1.2522	1.3644	1.4176	1.4175	0.5547	1.4434
image8	1.6283	1.8149	1.7951	1.7955	1.0847	1.7846
image9	1.3680	1.5673	1.6281	1.6284	1.1565	1.5616
image10	1.3925	1.6286	1.4651	1.4639	1.2000	1.6076
image11	1.4546	1.7123	1.7165	1.7184	1.3807	1.8270
image12	1.2470	1.5279	1.6722	1.6726	0.7988	1.6587
image13	1.4597	1.6535	1.5479	1.5456	0.9241	1.6730
image14	1.3613	1.6090	1.7079	1.7085	1.1727	1.7245
image15	1.4532	1.6889	1.6190	1.6193	1.1113	1.6955
image16	1.6060	1.7707	1.6479	1.6462	1.0506	1.8425
image17	1.7355	1.8985	1.8179	1.8164	1.0140	1.9246
image18	1.5652	1.7909	1.7982	1.7982	0.9778	1.8951
image19	1.6343	1.6932	1.5337	1.5339	1.0281	1.7143
image20	0.5354	0.9482	1.3457	1.3440	0.7305	1.5176
image21	1.2081	1.6072	1.7358	1.7361	0.9740	1.6182

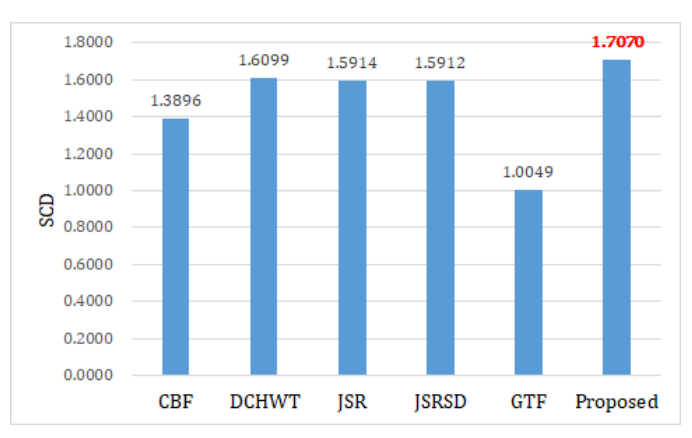


Fig. 11. The average values of SCD for fusion methods.

TABLE III THE  $SSIM_a$  values of the compared methods and the proposed method for 21 pairs source images.

Methods	CBF	DCHWT	JSR	JSRSD	GTF	Proposed
image1	0.6238	0.7483	0.5271	0.5271	0.6918	0.7618
image2	0.4986	0.6447	0.6240	0.6235	0.6111	0.6703
image3	0.5828	0.8259	0.6350	0.6350	0.8239	0.8773
image4	0.5831	0.7722	0.5903	0.5903	0.7613	0.8165
image5	0.5963	0.8062	0.4677	0.4677	0.7339	0.8337
image6	0.6172	0.7345	0.5045	0.5055	0.7321	0.7689
image7	0.6719	0.8319	0.5803	0.5813	0.8343	0.8628
image8	0.5236	0.5761	0.4542	0.4546	0.5027	0.6085
image9	0.6179	0.6566	0.4711	0.4725	0.6298	0.6891
image10	0.6304	0.7098	0.4463	0.4471	0.6728	0.7429
image11	0.6649	0.8381	0.7021	0.7036	0.8050	0.8590
image12	0.6497	0.7545	0.5830	0.5833	0.7008	0.7722
image13	0.5370	0.7061	0.5659	0.5657	0.6568	0.7323
image14	0.6989	0.7592	0.5209	0.5234	0.7425	0.7900
image15	0.5902	0.6883	0.4796	0.4803	0.6718	0.7229
image16	0.4575	0.6887	0.5764	0.5766	0.6606	0.7253
image17	0.5098	0.7273	0.6015	0.6008	0.6942	0.7728
image18	0.6882	0.8112	0.4368	0.4376	0.7795	0.8342
image19	0.6368	0.7127	0.4956	0.4959	0.6369	0.7167
image20	0.5301	0.6230	0.5742	0.5741	0.6297	0.7119
image21	0.6821	0.7421	0.5187	0.5206	0.7320	0.7928

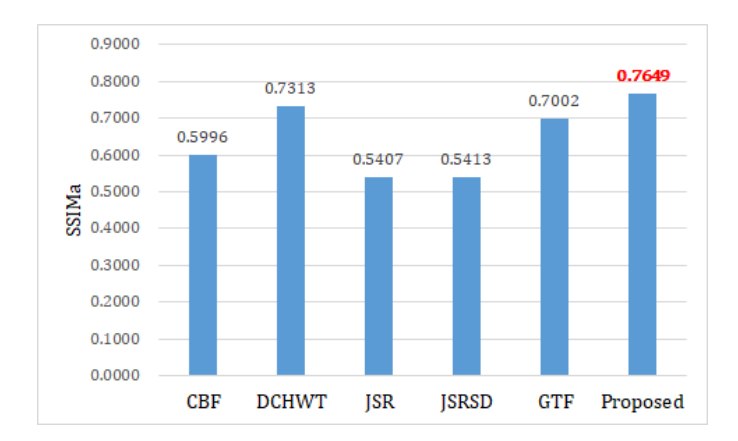


Fig. 12. The average values of  $SSIM_a$  for fusion methods

value are indicated in red. As we can see, the proposed method has all the best values in  $N_{abf}$  and  $SSIM_a$ . For the values of SCD, the proposed method has 15 best values and 2 second-best values. And for the average values of  $N_{abf}$ , SCD and  $SSIM_a$ , the proposed method also has all the best values, as shown in Fig.(10-12).

These values indicate that the fused images which are obtained by the proposed method are more natural and contain less artificial information. From objective evaluation, our fusion method has better fusion performance than those compared methods.

# V. CONCLUSION

In this paper, we proposed a simple and effective infrared and visible image fusion method based on latent low-rank representation. Firstly, the source images are decomposed into low-rank parts and saliency parts which contain global structure and local structure information, respectively. Then the fused low-rank part and saliency part are obtained by weighted-average strategy, and we choose different weight value for these two parts. Finally, the fused image is reconstructed by adding the fused low-rank part and the fused saliency part. We use both subjective and objective methods to evaluate the proposed method, the experimental results show that the proposed method exhibits better performance than other compared methods

### REFERENCES

- [1] Shutao Li, Xudong Kang, Leyuan Fang, Jianwen Hu, Haitao Yin. Pixellevel image fusion: A survey of the state of the art. Information fusion, 33(2017): 100-112.
- [2] A. Ben Hamza, Y. He, H. Krim, A. Willsky, A multiscale approach to pixel-level image fusion, Integrated Computer-Aided Engineering 12 (2) (2005) 135-146.
- [3] S. Yang, M. Wang, L. Jiao, R. Wu, Z. Wang, Image fusion based on a new contourlet packet, Information fusion, 11 (2) (2010) 7884.
- [4] L. Wang, B. Li, L. Tian, EGGDD: an explicit dependency model for multi-modal medical image fusion in shift-invariant shearlet transform domain, Information fusion, 19(1) (2014) 2937.
- [5] Pang H, Zhu M, Guo L. Multifocus color image fusion using quaternion wavelet transform[C] International Congress on Image and Signal Processing. IEEE, 2013:543-546.
- [6] Luo X, Zhang Z, Zhang B, et al. Image fusion with contextual statistical similarity and nonsubsampled shearlet transform[J]. IEEE Sensors Journal, 2017, PP(99):1-1.
- [7] Bavirisetti D P, Dhuli R. Two-scale image fusion of visible and infrared images using saliency detection[J]. Infrared Physics & Technology, 2016, 76:52-64.
- [8] Yu Zhang, Xiangzhi Bai, Tao Wang. Boundary finding based multifocus image fusion through multi-scale morphological focus-measure. Information fusion, 35(2017): 81-101.
- [9] Zong J J, Qiu T S. Medical image fusion based on sparse representation of classified image patches[J]. Biomedical Signal Processing & Control, 2017, 34:195-205.
- [10] Lu X, Zhang B, Zhao Y, et al. The infrared and visible image fusion algorithm based on target separation and sparse representation[J]. Infrared Physics & Technology, 2014, 67:397-407.
- [11] Yin M, Duan P, Liu W, et al. A novel infrared and visible image fusion algorithm based on shift-invariant dual-tree complex shearlet transform and sparse representation[J]. Neurocomputing, 2016.
- [12] Liu C H, Qi Y, Ding W R. Infrared and visible image fusion method based on saliency detection in sparse domain[J]. Infrared Physics & Technology, 2017, 83:94102.
- [13] Liu Y, Chen X, Ward R, et al. Image Fusion With Convolutional Sparse Representation[J]. IEEE Signal Processing Letters, 2016, (99):1-1.
- [14] Gao R, Vorobyov S, Zhao H. Image Fusion With Cosparse Analysis Operator[J]. IEEE Signal Processing Letters, 2017, PP(99):1-1.
- [15] Liu G, Yan S. Latent Low-Rank Representation for subspace segmentation and feature extraction[C]// International Conference on Computer Vision. IEEE Computer Society, 2011:1615-1622.
- [16] Liu G, Lin Z, Yu Y. Robust Subspace Segmentation by Low-Rank Representation[C]// International Conference on Machine Learning. DBLP, 2010:663-670.
- [17] Ma J, Zhou Z, Wang B, et al. Infrared and visible image fusion based on visual saliency map and weighted least square optimization[J]. Infrared Physics & Technology, 2017, 82:8-17.
- [18] B. K. Shreyamsha Kumar. Image fusion based on pixel significance using cross bilateral filter. Signal, Image and Video Processing, pp. 1-12, 2013.
- [19] B. K. Shreyamsha Kumar. Multifocus and Multispectral Image Fusion based on Pixel Significance using Discrete Cosine Harmonic Wavelet Transform. Signal, Image and Video Processing, 2012.
- [20] Zhang A Q, Fu Y, Li H, et al. Dictionary learning method for joint sparse representation-based image fusion[J]. Optical Engineering, 2013, 52(5):7006.
- [21] Ma J, Chen C, Li C, et al. Infrared and visible image fusion via gradient transfer and total variation minimization[J]. Information Fusion, 2016, 31(C):100-109.
- [22] V. Aslantas and E. Bendes. A new image quality metric for image fusion: The sum of the correlations of differences[J]. AEU - International Journal of Electronics and Communications, vol. 69/12, pp. 1890-1896, 2015.

**Hui Li** received the B.E. degree in School of Internet of Things Engineering from Jiangnan University, China. He is currently a master student in the School of Internet of Things Engineering, Jiangnan University. His research interests include image fusion and machine learning.

Xiao-Jun Wu received the B.S. degree in mathematics from Nanjing Normal University, Nanjing, China, in 1991, and the M.S. degree and Ph.D. degree in pattern recognition and intelligent system from the Nanjing University of Science and Technology, Nanjing, in 1996 and 2002, respectively. From 1996 to 2006, he taught at the School of Electronics and Information, Jiangsu University of Science and Technology, where he was promoted to Professor. He has been with the School of Information Engineering, Jiangnan University, since 2006, where he is a Professor of Computer Science and Technology. He was a Visiting Researcher with the Centre for Vision, Speech, and Signal Processing, University of Surrey, U.K., from 2003 to 2004. He has published over 150 papers. His current research interests include pattern recognition, computer vision, and computational intelligence. He was a Fellow of the International Institute for Software Technology, United Nations University, from 1999 to 2000. He was a recipient of the Most Outstanding Postgraduate Award from the Nanjing University of Science and Technology.